Since January 2020 Elsevier has created a COVID-19 resource centre with free information in English and Mandarin on the novel coronavirus COVID-19. The COVID-19 resource centre is hosted on Elsevier Connect, the company's public news and information website.

Bioorganic Chemistry 114 (2021) 105117

Contents lists available at ScienceDirect

Bioorganic Chemistry

journal homepage: www.elsevier.com/locate/bioorg

New quinoline-triazole conjugates: Synthesis, and antiviral properties against SARS-CoV-2

Israa A. Seliem [a,b], Siva S. Panda [a,*], Adel S. Girgis [c], Yassmin Moatasim [d], Ahmed Kandeil [d], Ahmed Mostafa [d], Mohamed A. Ali [d], Eman S. Nossier [e], Fatma Rasslan [f], Aladdin M. Srour [g], Rajeev Sakhuja [h], Tarek S. Ibrahim [i,b], Zakaria K.M. Abdel-samii [b], Amany M.M. Al-Mahmoudy [b]

[a] Department of Chemistry and Physics, Augusta University, Augusta, GA 30912, USA
[b] Department of Pharmaceutical Organic Chemistry, Faculty of Pharmacy, Zagazig University, Zagazig 44519, Egypt
[c] Department of Pesticide Chemistry, National Research Centre, Dokki, Giza 12622, Egypt
[d] Center of Scientific Excellence for Influenza Viruses, National Research Centre, Giza 12622, Egypt
[e] Department of Pharmaceutical Medicinal Chemistry and Drug Design, Faculty of Pharmacy (Girls), Al-Azhar University, Cairo, Egypt
[f] Department of Microbiology and Immunology, Faculty of Pharmacy (Girls), Al Azhar University, Cairo, Egypt
[g] Department of Therapeutic Chemistry, National Research Centre, Dokki, Giza 12622, Egypt
[h] Department of Chemistry, Birla Institute of Technology and Science, Pilani, India
[i] Department of Pharmaceutical Chemistry, Faculty of Pharmacy, King Abdulaziz University, Jeddah 21589, Saudi Arabia

ARTICLE INFO

Keywords:
Quinoline
Triazole
Click chemistry
SARS-CoV-2
Molecular docking

ABSTRACT

At present therapeutic options for severe acute respiratory syndrome coronavirus-2 (SARS-CoV-2) are very limited. We designed and synthesized three sets of small molecules using quinoline scaffolds. A series of quinoline conjugates (10a-l, 11a-c, and 12a-e) by incorporating 1,2,3-triazole were synthesized *via* a modified microwave-assisted click chemistry technique. Among the synthesized conjugates, 4-((1-(2-chlorophenyl)-1*H*-1,2,3-triazol-4-yl)methoxy)-6-fluoro-2-(trifluoromethyl)quinoline (10g) and 6-fluoro-4-(2-(1-(4-methoxyphenyl)-1*H*-1,2,3-triazol-4-yl)ethoxy)-2-(trifluoromethyl)quinoline (12c) show high potency against SARS-CoV-2. The selectivity index (SI) of compounds 10g and 12c also indicates the significant efficacy compared to the reference drugs.

1. Introduction:

In December 2019, an unknown viral infection was identified in a local fish and wild animal market of Wuhan city (China) [1]. Since then, the virus has rapidly spread across mainland China followed by the rest of the world [2,3]. On Feb 11, 2020, the WHO identified the virus as the severe acute respiratory syndrome coronavirus-2 (SARS-CoV-2). The viral infection disease is called as 2019-new coronavirus disease (COVID-19), and in March 2020 declared the coronavirus outbreak a global pandemic [4]. As of April 2021, COVID-19 has affected more than 152 million people with 3.18 million deaths worldwide.

As of now, there is no potential antiviral drug available for the treatment of COVID-19. However, a few vaccines have received approval from FDA to control the pandemic. The drug repurposing approach was considered the most accessible pathway for exploring drugs to control the global pandemic. Several drugs that were considered for repurposing to control the COVID-19 pandemic include chloroquine (CQ) and hydroxychloroquine (HCQ) (Fig. 1). These exhibited promising responses accompanied with serious side effects (ventricular arrhythmias, retinopathy, QT prolongation, or cardiac-related toxicity) [5–11]. Recently, a few quinolone-based small molecules reported their antiviral properties against SARS-CoV-2 [12–20].

New drug development is expensive, time-consuming, and challenging processes. In the current scenario, molecular hybridization of bioactive moieties is a powerful and attractive rational drug design strategy for new drug development because of several advantages such as a) to achieve selectivity; b) gain desired activity; c) multiple pharmacological targets; d) lower possible cytotoxicity. Our group has actively engaged in developing drug conjugates and hybrid conjugates by this approach [21–26].

In the present study, we have designed and synthesized a set of novel quinoline-triazole conjugates with potential antiviral properties against

* Corresponding author.
E-mail address: sipanda@augusta.edu (S.S. Panda).

https://doi.org/10.1016/j.bioorg.2021.105117
Received 7 April 2021; Received in revised form 8 May 2021; Accepted 19 June 2021
Available online 23 June 2021

SARS-CoV-2 using the 'click' chemistry approach employing various azides and the alkyne component of the propargyl linked quinolines. We considered the quinoline scaffold from the repurposed drugs (chloroquine and hydroxychloroquine) and triazole because of their importance in the drug development process and well-known for diversified biological properties [27–31]. Besides, the presence of electronegative fluorine atoms may alter the physicochemical properties of the molecule significantly. This may improve the stability, reducing the cytotoxicity, in addition to enhancing the overall therapeutic efficacy in our designed molecules [32].

2. Results and discussion

The synthetic protocol was developed for the synthesis of the targeted quinoline-triazole conjugates (Fig. 2) by adopting the well-established Cu-mediated click chemistry of alkynes **5**, **6,** and **8** with varied azides **10**. The precursor alkynes **5**, **6**, and **8** were synthesized by treating a solution of 6-(un)substituted-2-(trifluoromethyl)quinolin-4 (1*H*)-ones **3** in DMF with propargyl bromide (**4**) or 4-bromobut-1-yne (**7**) in the presence of potassium carbonate (K_2CO_3) at room temperature [33]. (Scheme 1). The azides of aromatic amines **1b–f** were synthesized using the previously reported method [25].

2.1. Synthesis of alkynes 5, 6, and 8

A solution of compounds **3a–d** in DMF on reaction with propargyl bromide (**4**) or 4-bromobut-1-yne (**7**) in the presence of potassium carbonate (K_2CO_3) at 20 °C for 6 h gave predominately *O*-substituted quinolines. However, in the case of **3a** and **3c** on treatment with propargyl bromide **4**, we got both *N*-substituted quinolones and *O*-substituted quinolines in a good ratio, which were isolated by column chromatography (**5a**,**b,** and **6a**,**b**). We also observed the formation of *N*-substituted quinolones as a minor product when we treated 4-bromobut-1-yne (**7**) with **3a–d**. The formation of *O*-substituted quinolones is move favored over *N*-substituted quinolines because of the steric and electronic properties of the CF_3 group. The detailed investigation was reported by Raić-Malić and coworkers [34].

2.2. Synthesis of triazole-quinoline conjugates

Alkynes **5**, **6,** and **8** were treated with aromatic azides **9** adopting a modified click chemical technique in presence of $CuSO_4{\cdot}5H_2O$ and sodium D-isoascorbate in *n*-butanol–water mixture under microwave irradiation for 2 h at 100 °C to afford the desired corresponding conjugates **10a–l**, **11a–c** and **12a–e** in good yields (Scheme 2). The reactions do work at room temperature but never go to completion even after 3 days. Our optimized reaction condition able to complete the reaction in 2 h. All the synthesized compounds were fully characterized by spectroscopic techniques.

2.3. Antiviral properties

The antiviral properties of the synthesized conjugates (**10**, **11,** and **12**) against SARS-CoV-2 were determined by the standard technique [35–37]. Table 1 exhibits the antiviral properties of the tested compounds and standard references (CQ, HCQ) used expressed as IC_{50} (concentration necessary for 50% reduction of virus-induced cytopathic effect (CPE) compared to the virus control experiment). We have also determined the CC_{50} (concentration necessary for 50% growth normal cell line "VERO-E6" inhibition compared to the control experiment) for all the synthesized conjugates (Fig. 3). We calculated the selectivity (therapeutical) index (SI), which is the ratio of CC_{50} relative to IC_{50} of the tested conjugate. From the observed biological properties (Table 1), it has been noticed that conjugate **10g** is superior among all the tested agents revealing potent antiviral inhibition with high selectivity index relative to the standard references used (IC_{50} = 0.060, 0.0227, 0.0328 mM; CC_{50} = 1.585, 0.3777, 0.356 mM, SI = 26.42, 16.64, 10.85; corresponding to **10g**, CQ and HCQ, respectively). Conjugate **12c** also reveals enhanced selectivity index relative to the standard references used with milder antiviral potency (IC_{50} = 0.204, CC_{50} = 3.493 mM, SI = 17.12). Additionally, compounds **10i**, **11a**, **11c**, **12a,** and **12e** also show promising biological properties with a considerable selectivity index (SI = 4.51–3.15).

Some qualitative structure–activity relationship could be assigned based on observed antiviral properties. The fluoroquinolinyl conjugates show enhanced antiviral properties than the unsubstituted conjugates as exhibited in pairs **10f**/**10b** (IC_{50} = 2.648, 8.466 mM), **10g**/**10d** (IC_{50} = 0.060, 0.768 mM), **10h**/**10e** (IC_{50} = 4.471, 85.576 mM) and **12c**/**12a** (IC_{50} = 0.204, 0.7678 mM). Probably the fluorine atoms play important role in enhancing the antiviral properties. Moreover, the *o*-chlorophenyl triazolyl conjugates reveal higher antiviral properties than the *o*-methoxyphenyl analogues as shown in pairs **10d**/**10e** (IC_{50} = 0.768, 85.576 mM) and **10g**/**10h** (IC_{50} = 0.060, 4.471 mM). Additionally, molecular modeling can estimate the parameters/functional groups necessary for optimizing antiviral properties.

2.4. Molecular docking study

Molecular docking is one of the most important computational techniques widely accessible in medicinal chemical studies for many

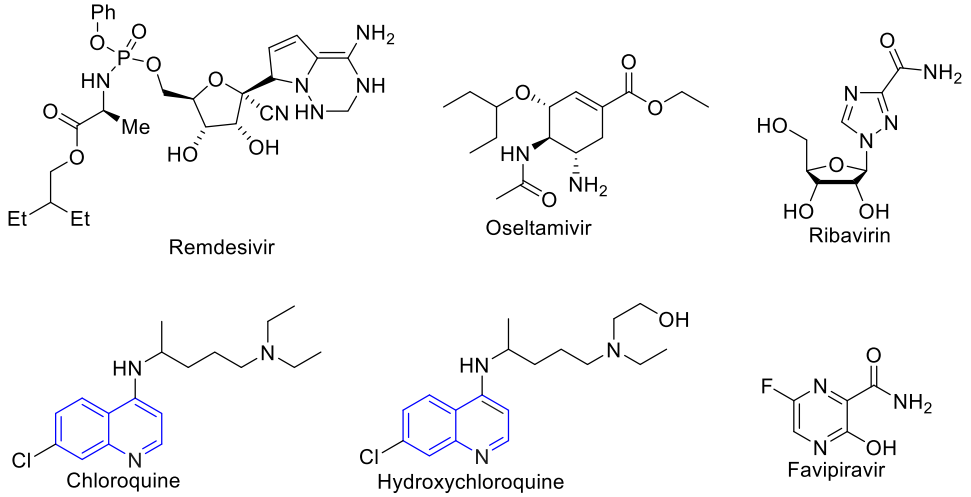

Fig. 1. Examples of repurposing drugs for COVID-19.

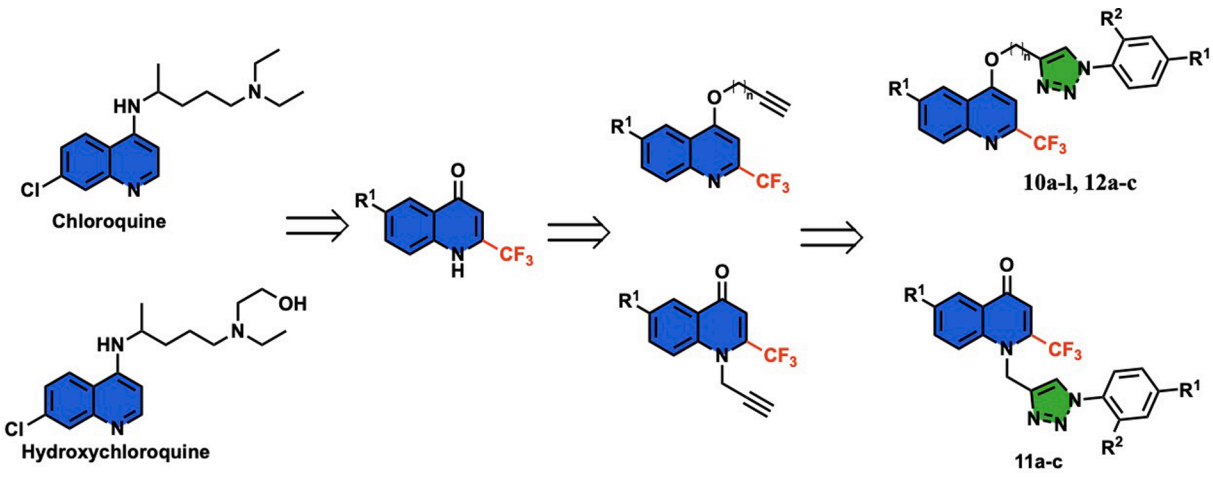

Fig. 2. Designing of quinoline-triazole conjugates.

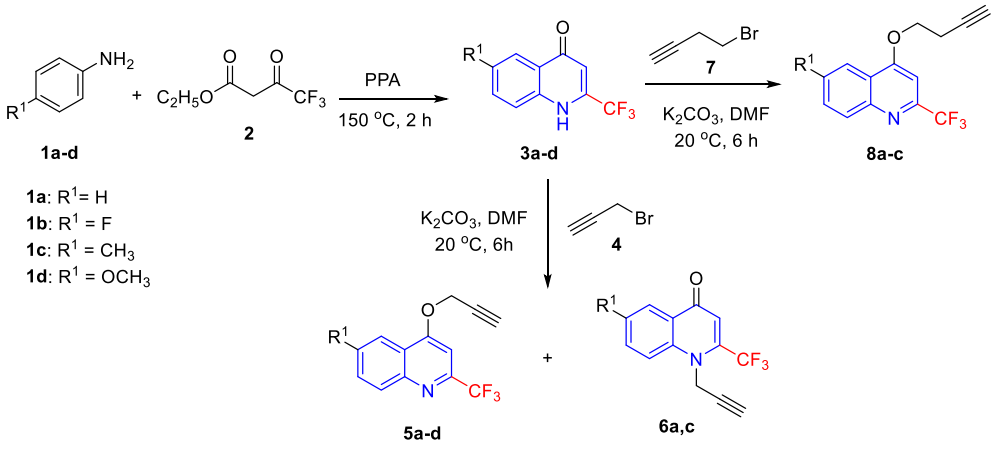

Scheme 1. Synthesis of alkynes **5**, **6,** and **8**.

purposes of which, determining/predicting the mode of action of an agent and explaining the observed bio-properties. The tested compounds against SARS-CoV-2 were subjected for molecular docking study utilizing PDB ID: 6LU7 "SARS-CoV-2 main protease (M^{pro}) with an inhibitor N3" [38,39]. Discovery Studio 2.5 software was used (CDOCKER, force field: CHARMm, ligand partial charge method: MMFF).

From the docking observations (Supplementary Figs. S1 and S2), it has been noticed that chloroquine and hydroxychloroquine show hydrogen bonding due to the diethylamino nitrogen interaction with GLU166 (which is one of the amino acids revealing interaction with the co-crystallized ligand "N3 inhibitor" in the PDB: 6LU7), and docking scores −46.2, −42.3 kcal mol^{-1} for chloroquine and hydroxychloroquine, respectively. These observations are comparable to their antiviral properties observed (IC_{50} = 0.0227, 0.0328 mM, respectively). Compounds **10g** and **12c**, which are the most effective antiviral agents synthesized (IC_{50} = 0.060, 0.204 mM, respectively) reveal behavior due to hydrogen bonding observation. Where the triazolyl nitrogen has hydrogen bonding interaction with the same amino acid (GLU166). Additionally, the promising agents synthesized **10d**, **10i**, **12a** and **12e** (IC_{50} = 0.768, 0.331, 0.7678, 0.930 mM, respectively) also exhibit similar docking observations. However, other analogs show good docking scores due to false alignment in the protein active site "interaction with amino acid(s) other than those overlapped with the co-crystallized ligand". These findings support the experimentally observed weak antiviral properties (e.g. compounds **10c** and **10e** of IC_{50} = 113.5, 85.6 mM and docking scores = -37.9, −38.5 kcal/mol, respectively).

2.5. Conclusion

In conclusion, we have synthesized three sets of triazole incorporated quinolone conjugates in good yields by an optimized facile reaction condition. Some conjugates showed promising antiviral activity against SARS-CoV-2. Compound **10g** and **12c** found the most effective agents for the SARS-CoV-2. The selectivity index (SI) of compounds also indicates significant efficacy compared to the reference drugs. We believe the initial investigation and the important scaffold could be further used as resources for the development of potential drug candidates for SARS-CoV-2.

3. Experimental section

3.1. Chemistry

Melting points were determined on a capillary point apparatus equipped with a digital thermometer. NMR spectra were recorded in $CDCl_3$, DMSO-d_6, on Bruker NMR spectrometer operating at 500 MHz for ^1H (with TMS as an internal standard) and 125 MHz for ^{13}C. High-resolution mass spectra were recorded with TOF analyzer spectrometer by using electron spray mode. All microwave-assisted reactions were carried out with a single-mode cavity Discover Microwave Synthesizer (CEM Corporation, NC). The reaction mixtures were transferred into a 10 mL glass pressure microwave tube equipped with a magnetic stirrer bar. The tube was closed with a silicon septum and the reaction mixture was subjected to microwave irradiation (Discover mode; run

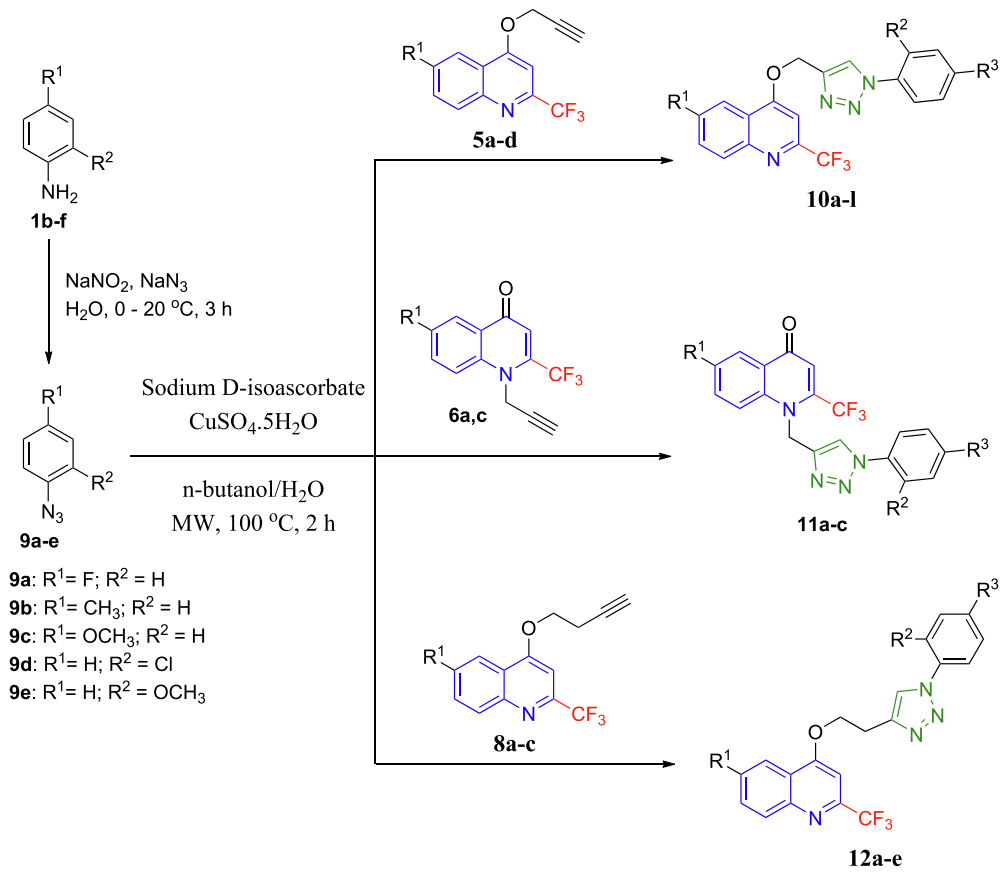

Scheme 2. Triazole-quinoline conjugates **10a-l**, **11a-c**, **12a-e**.

Table 1
Antiviral properties of the quinine-triazole conjugates **10, 11,** and **12** against SARS-CoV-2.

Entry	Compound	R^1	R^2	R^3	IC_{50} (mM)[a]	CC_{50} (mM)[b]	SI[c]
1	**10a**	H	H	F	0.531	2.676	5.04
2	**10b**	H	H	CH_3	8.466	4.114	0.49
3	**10c**	H	H	OCH_3	113.504	3.104	0.03
4	**10d**	H	Cl	H	0.768	2.192	2.85
5	**10e**	H	OCH_3	H	85.576	2.183	0.03
6	**10f**	F	H	CH_3	2.648	4.524	1.71
7	**10g**	F	Cl	H	**0.060**	**1.585**	**26.42**
8	**10h**	F	OCH_3	H	4.471	3.408	0.76
9	**10i**	CH_3	Cl	H	0.331	1.494	4.51
10	**10j**	CH_3	OCH_3	H	nd	nd	nd
11	**10k**	OCH_3	H	F	3.106	4.170	1.34
12	**10l**	OCH_3	H	CH_3	1.607	1.050	0.65
13	**11a**	H	H	OCH_3	1.310	4.831	3.69
14	**11b**	H	OCH_3	H	nd	nd	nd
15	**11c**	CH_3	H	OCH_3	0.5265	1.659	3.15
16	**12a**	H	H	OCH_3	0.7678	2.960	3.86
17	**12b**	F	H	F	6.609	3.650	0.55
18	**12c**	F	H	OCH_3	**0.204**	**3.493**	**17.12**
19	**12d**	F	OCH_3	H	0.860	0.982	1.14
20	**12e**	CH_3	H	OCH_3	0.930	2.964	3.19
21	**CQ**				0.0227	0.3777	16.64
22	**HCQ**				0.0328	0.356	10.85

nd: not done.

[a] IC_{50}: Concentration necessary for 50% reduction of virus-induced cytopathic effect (CPE) compared to the virus control experiment.

[b] CC_{50}: Half maximal cytotoxic concentration for the normal cell line (VERO-E6) inhibition compared to the control experiment.

[c] SI (Selectivity index/therapeutical index): $\frac{CC_{50}}{IC_{50}}$.

time: 60 s; Power Max-cooling mode).

3.1.1. General procedure for the synthesis of O-alkynyl-oxyquinolines 5a-d and N-alkynyl-oxyquinolines 6a,c [26,33]

To a suspension of corresponding quinolone **3a–d** (1 equiv.) in *N*, *N*-dimethylformamide (DMF; 10 mL), K_2CO_3 (1.5 equiv.) was added. After

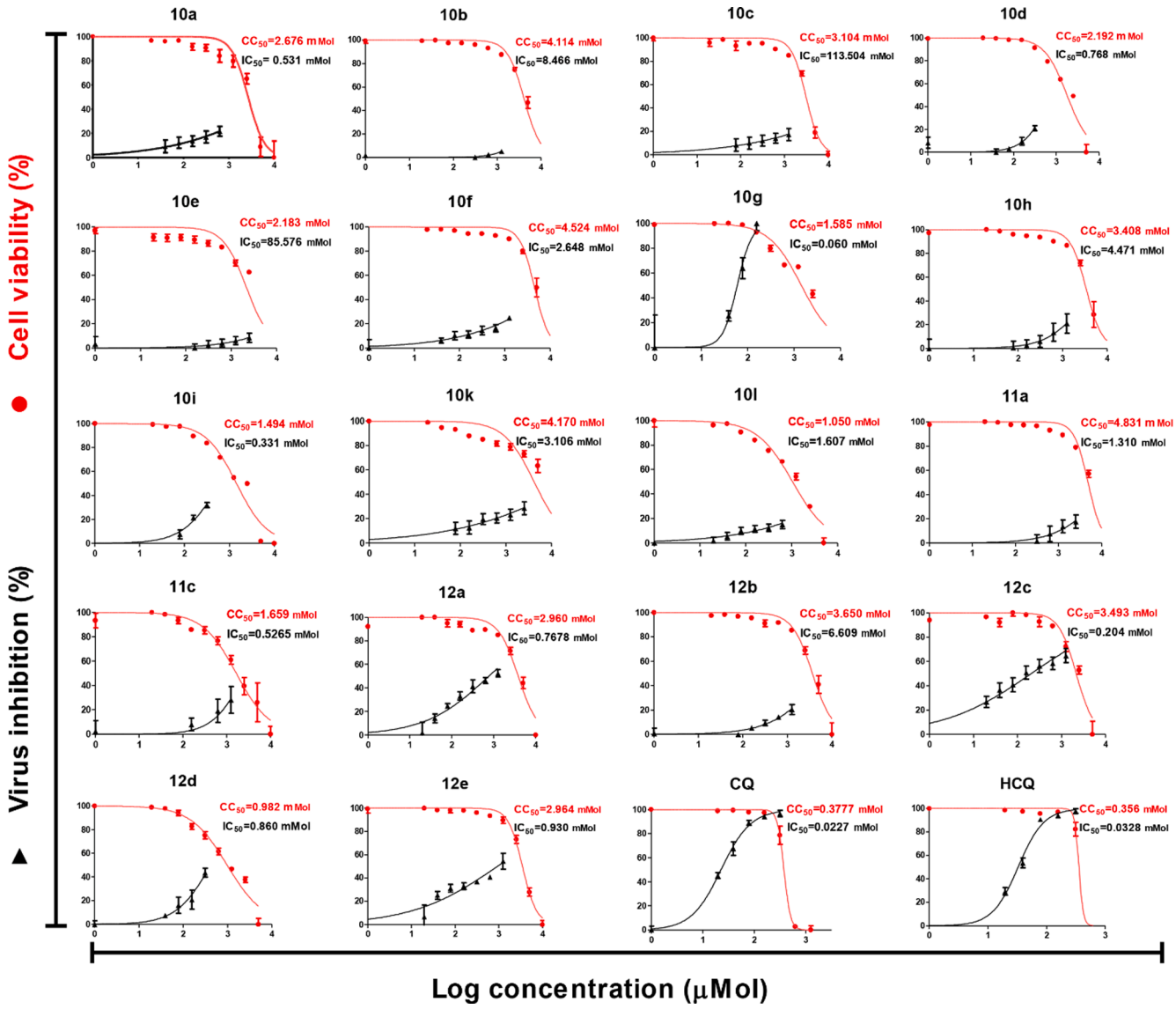

Fig. 3. Dose-response curves for the tested compounds against SARS-CoV-2.

stirring for 30 min, propargyl bromide **4** (1 equiv.) was added and the reaction mixture was stirred for 6 h. The solvent was removed under reduced pressure and the crude residue was purified by column chromatography. These compounds were characterized by comparing their spectroscopic data to the reported ones [26,33].

3.1.2. General procedure for the synthesis of synthesis O-alkynyl-quinolines 8a-c [33]

To a suspension of corresponding quinolone **3a–d** (1 equiv.) in *N*, *N*-dimethylformamide (DMF; 10 mL), K_2CO_3 (1.5 equiv.) was added. After stirring for 30 min, 4-bromobut-1-yne **7** (1 equiv.) was added and the reaction mixture was subjected to microwave irradiations for 6 h. The crude mixture was diluted with water than solid formed filtered off and crystallized from ethanol. These compounds were characterized by comparing their spectroscopic data to the reported ones [28].

3.1.3. General procedure for the synthesis of quinoline-triazole conjugates

To a solution of quinoline (1 equiv.) in *n*-butanol/H_2O (2: 1) (3 mL), $CuSO_4$ (0.05 equiv.), and sodium D-isoascorbate monohydrate (0.15 equiv.) was added at room temperature. To this mixture, aryl azide (1.5 mmol) was added and the reaction mixture was subjected to microwave irradiations at 250 W for 2 h. The crude mixture was diluted with water then extracted with EtOAc and the combined organic layer was dried over sodium sulfate, concentrated in a vacuum, and purified through column chromatography to give the pure quinoline-triazole derivatives in good yields.

*3.1.3.1. 4-((1-(4-Fluorophenyl)-1H-1,2,3-triazol-4-yl)methoxy)-2-(trifluoromethyl)quinoline (**10a**).* White microcrystals, m.p. 173–175 °C, yield 46% (0.28 g). IR: ν_{max}/cm^{-1} 3052, 2923, 1574, 1515, 1378, 1233, 831, 763; ^{1}H NMR ($CDCl_3$) δ: 8.22 (d, J = 8.0 Hz, 1H), 8.14 (d, J = 8.5 Hz, 1H), 8.10 (s, 1H), 7.81–7.75 (m, 1H), 7.73 (dd, J = 9.0, 4.6 Hz, 2H), 7.59 (t, J = 7.6 Hz, 1H), 7.28 (s, 1H), 7.24 (t, J = 4.0 Hz, 1H), 7.21 (s, 1H), 5.56 (s, 2H). ^{13}C NMR ($CDCl_3$) δ: 163.9, 162.5, 161.9, 149.4, 149.1, 148.4, 143.3, 133.3, 131.3, 129.9, 127.9, 123.0, 122.9, 122.1, 121.8, 117.2, 117.0, 97.4, 62.7. HRMS *m/z* for $C_{19}H_{12}F_4N_4O$ $[M+H]^+$ Calcd. 389.1020. Found: 389.1013.

*3.1.3.2. 4-((1-(p-Tolyl)-1H-1,2,3-triazol-4-yl)methoxy)-2-(trifluoromethyl)quinoline (**10b**).* White microcrystals, m.p. 172–174 °C, yield 54% (0.32 g). IR: ν_{max}/cm^{-1} 3050, 2930, 1575, 1514, 1372, 1252, 817, 770; ^{1}H NMR ($CDCl_3$) δ: 8.23 (d, J = 8.3 Hz, 1H), 8.15–8.10 (m, 2H), 7.77 (t, J = 7.7 Hz, 1H), 7.64–7.54 (m, 3H), 7.32 (d, J = 8.1 Hz, 2H), 7.28 (s, 1H), 5.55 (s, 2H), 2.41 (s, 3H).^{13}C NMR ($CDCl_3$) δ: 162.2,

149.3, 149.1, 148.4, 139.6, 134.7, 133.0, 131.3, 130.6, 129.8, 127.9, 125.6, 122.8, 122.1, 121.8, 120.8, 120.6, 97.4, 62.8, 21.3. HRMS *m/z* for $C_{20}H_{15}F_3N_4O$ $[M+H]^+$ Calcd. 385.1271. Found: 385.1278.

*3.1.3.3. 4-((1-(4-Methoxyphenyl)-1H-1,2,3-triazol-4-yl)methoxy)-2-(trifluoromethyl)quinoline (**10c**).* White microcrystals, m.p. 180–182 °C, yield 54% (0.32 g). IR: ν_{max}/cm^{-1} 3050, 2980, 1591, 1515, 1370, 1252, 840, 771; ^1H NMR ($CDCl_3$) δ: 8.19 (d, $J = 8.3$ Hz, 1H), 8.13–8.05 (m, 2H), 7.74 (t, $J = 7.5$ Hz, 1H), 7.61 (d, $J = 8.5$ Hz, 2H), 7.55 (t, $J = 7.5$ Hz, 1H), 7.25 (d, $J = 6.2$ Hz, 1H), 6.99 (d, $J = 8.5$ Hz, 2H), 5.51 (s, 2H), 3.83 (s, 3H). ^{13}C NMR ($CDCl_3$) δ: 162.6, 160.3, 149.2, 148.9, 148.3, 142.8, 131.3, 130.3, 129.7, 127.8, 122.7, 122.5, 122.1, 121.9, 121.8, 120.6, 115.0, 97.3, 62.8, 55.8. HRMS *m/z* for $C_{20}H_{15}F_3N_4O_2$ $[M+H]^+$ Calcd. 401.1220. Found: 401.1224.

*3.1.3.4. 4-((1-(2-Chlorophenyl)-1H-1,2,3-triazol-4-yl)methoxy)-2-(trifluoromethyl)quinoline (**10d**).* White microcrystals, m.p. 200–202 °C, yield 44% (0.26 g). IR: ν_{max}/cm^{-1} 3079, 2979, 1574, 1530, 1369, 1274, 848, 788, 756; ^1H NMR ($CDCl_3$) δ: 8.40 (d, $J = 8.2$ Hz, 1H), 8.30 (t, $J =$ 8.5 Hz, 1H), 8.22 (s, 1H), 8.19 (d, $J = 8.4$ Hz, 1H), 7.74 (t, $J = 7.6$ Hz, 1H), 7.65–7-62 (m, $J = 10.7$, 3.9 Hz, 2H), 7.57–7.44 (m, 2H), 7.33 (s, 1H), 5.65 (s, 2H).^{13}C NMR ($CDCl_3$) δ: 162.6, 148.5, 142.2, 132.1, 131.3, 131.1, 130.7, 129.9, 129.8, 128.3, 128.0, 127.9, 125.6, 122.2, 121.9, 121.1, 108.1, 97.5, 62.8. HRMS *m/z* for: $C_{19}H_{12}ClF_3N_4O$ $[M+H]^+$ Calcd. 405.0724. Found: 405.0724.

*3.1.3.5. 4-((1-(2-Methoxyphenyl)-1H-1,2,3-triazol-4-yl)methoxy)-2-(trifluoromethyl)quinoline (**10e**).* White microcrystals, m.p. 179–181 °C, yield 61% (0.37 g). IR: ν_{max}/cm^{-1} 3100, 2931, 1576, 1512, 1368, 1249, 831, 756; ^1H NMR ($CDCl_3$) δ: 8.23 (d, $J = 8.5$ Hz, 1H), 8.15 (d, $J = 8.5$ Hz, 1H), 8.07 (s, 1H), 7.77 (t, $J = 8.1$ Hz, 1H), 7.63 (d, $J = 9.0$ Hz, 2H), 7.58 (t, $J = 7.6$ Hz, 1H), 7.29 (s, 1H), 7.01 (d, $J = 9.0$ Hz, 2H), 5.55 (s, 2H), 3.85 (s, 3H).^{13}C NMR ($CDCl_3$) δ: 162.9, 151.2, 131.4, 131.3, 130.6, 129.7, 128.3, 128.0, 127.9, 126.2, 125.9, 125.7, 122.3, 122.2, 121.9, 121.6, 112.5, 97.5, 62.9, 56.2. HRMS *m/z* for: $C_{20}H_{15}F_3N_4O_2$ $[M+H]$ + Calcd. 401.1220. Found: 401.1217.

*3.1.3.6. 6-Fluoro-4-((1-(p-tolyl)-1H-1,2,3-triazol-4-yl)methoxy)-2-(trifluoromethyl)quinoline (**10f**).* White microcrystals, m.p. 170–172 °C, yield 75% (0.46 g). IR: ν_{max}/cm^{-1} 3100, 2925, 1577, 1517, 1478, 1277, 815, 717; ^1H NMR ($CDCl_3$) δ: 8.18–8.09 (m, 2H), 7.81 (dd, $J = 9.2$, 2.7 Hz, 1H), 7.62 (d, $J = 8.4$ Hz, 2H), 7.52 (td, $J = 9.2$, 2.8 Hz, 1H), 7.38–7.26 (m, 3H), 5.55 (s, 2H), 2.42 (s, 3H).^{13}C NMR ($CDCl_3$) δ: 162.5, 160.5, 145.4, 142.7, 139.7, 134.7, 132.6, 132.5, 130.6, 122.9, 122.7, 121.8, 121.6, 121.4, 120.8, 106.3, 106.1, 97.9, 62.9, 21.3. HRMS *m/z* for $C_{20}H_{14}F_4N_4O$ $[M+H]^+$ Calcd. 403.1177. Found: 403.1176.

*3.1.3.7. 4-((1-(2-Chlorophenyl)-1H-1,2,3-triazol-4-yl)methoxy)-6-fluoro-2-(trifluoromethyl)quinoline (**10g**).* White microcrystals, m.p. 174–176 °C, yield 79% (0.48 g). IR: ν_{max}/cm^{-1} 3050, 2930, 1600, 1574, 1518, 1478, 1233, 852, 761; ^1H NMR ($CDCl_3$) δ: 8.18–8.11 (m, 2H), 7.82 (dd, $J = 9.1$, 2.7 Hz, 1H), 7.66 (dd, $J = 6.4$, 3.0 Hz, 1H), 7.59 (dd, $J =$ 7.3, 2.0 Hz, 1H), 7.55–7.44 (m, 3H), 7.31 (s, 1H), 5.59 (s, 2H).^{13}C NMR ($CDCl_3$) δ: 162.1, 160.6, 145.5, 142.0, 134.8, 132.6, 132.5, 131.3, 131.1, 128.8, 128.3, 128.0, 126.0, 121.7, 121.5, 106.3, 106.1, 97.9, 62.9. HRMS *m/z* for $C_{19}H_{11}ClF_4N_4O$ $[M+H]^+$ Calcd. 423.0630. Found: 423.0631.

*3.1.3.8. 6-Fluoro-4-((1-(2-methoxyphenyl)-1H-1,2,3-triazol-4-yl) methoxy)-2-(trifluoromethyl)quinoline (**10h**).* White microcrystals, m.p. 154–156 °C, yield 67% (0.41 g). IR: ν_{max}/cm^{-1} 3100, 2980, 1599, 1506, 1478, 1249, 837; ^1H NMR ($CDCl_3$) δ: 8.31 (s, 1H), 8.12 (dd, $J = 9.2$, 5.2 Hz, 1H), 7.81–7.79 (m, 2H), 7.52–7.46 (m, 2H), 7.32 (s, 1H), 7.09 (dd, J = 13.0, 8.0 Hz, 2H), 5.55 (s, 2H), 3.87 (s, 3H).^{13}C NMR ($CDCl_3$) δ: 162.2, 160.4, 151.1, 145.3, 141.3, 132.4, 132.3, 130.6, 128.2, 127.9, 126.1, 125.9, 125.5, 121.5, 121.3, 112.5, 106.1, 97.9, 62.9, 56.2. HRMS *m/z* for $C_{20}H_{14}F_4N_4O_2$ $[M+H]^+$ Calcd. 419.1126. Found: 419.1123.

*3.1.3.9. 4-((1-(2-Chlorophenyl)-1H-1,2,3-triazol-4-yl)methoxy)-6-methyl-2-(trifluoromethyl)quinoline (**10i**).* White microcrystals, m.p. 179–181 °C, yield 78% (0.47 g). IR: ν_{max}/cm^{-1} 3000, 2980, 1575, 1495, 1372, 1251, 847, 767; ^1H NMR ($CDCl_3$) δ: 8.15–8.09 (m, 2H), 7.81 (dd, $J = 9.2$, 2.7 Hz, 1H), 7.62 (d, $J = 8.4$ Hz, 2H), 7.52 (td, $J = 9.2$, 2.8 Hz, 1H), 7.33–7.31(m, 3H),5.55 (s, 2H), 2.42 (s, 3H). ^{13}C NMR ($CDCl_3$) δ: 162.0, 154.4, 147.0, 138.2, 134.9, 134.4, 133.6, 131.3, 131.1, 130.4, 129.6, 128.8, 128.3, 128.0, 125.6, 120.1, 119.7, 97.4, 62.7, 22.1. HRMS *m/z* for $C_{20}H_{14}ClF_3N_4O$ $[M+H]^+$ Calcd. 419.0881. Found: 419.0883.

*3.1.3.10. 4-((1-(2-Methoxyphenyl)-1H-1,2,3-triazol-4-yl)methoxy)-6-methyl-2-(trifluoromethyl)quinoline (**10j**).* White microcrystals, m.p. 185–187 °C, yield 65% (0.40 g). IR: ν_{max}/cm^{-1} 3070, 2968, 1574, 1507, 1374, 1251, 830, 762; ^1H NMR ($CDCl_3$) δ: 8.30 (s, 1H), 8.15 (d, $J = 8.6$ Hz, 1H), 8.02 (s, 1H), 7.83 (dd, $J = 7.9$, 1.5 Hz, 1H), 7.62 (dd, $J = 8.7$, 1.3 Hz, 1H), 7.44 (td, $J = 8.4$, 1.6 Hz, 1H), 7.30 (s, 1H), 7.15–7.07 (m, 2H), 5.58 (s, 2H), 3.89 (s, 3H), 2.53 (s, 3H). ^{13}C NMR ($CDCl_3$) δ: 162.4, 151.2, 146.7, 141.6, 138.3, 133.7, 131.3, 131.1, 130.6, 129.3, 126.2, 125.9, 125.6, 121.9, 121.6, 121.1, 112.5, 97.5, 62.9, 56.2, 22.1. HRMS *m/z* for $C_{21}H_{17}F_3N_4O_2$ $[M+Na]^+$ Calcd. 415.1376. Found: 415.1383.

*3.1.3.11. 4-((1-(4-Fluorophenyl)-1H-1,2,3-triazol-4-yl)methoxy)-6-methoxy-2-(trifluoromethyl)quinoline (**10k**).* White microcrystals, m.p. 190–192 °C, yield 75% (0.46 g). IR: ν_{max}/cm^{-1} 3100, 2923, 1590, 1513, 1438, 1373, 1229, 840, 724; ^1H NMR ($CDCl_3$) δ: 8.10 (s, 1H), 8.05–7.96 (m, 1H), 7.71 (dd, $J = 8.9$, 4.5 Hz, 2H), 7.42–7.34 (m, 2H), 7.22–7.20 (m, 3H), 5.52 (s, 2H), 3.89 (s, 3H). ^{13}C NMR ($CDCl_3$) δ: 163.8, 161.8, 161.2, 159.1, 146.7, 146.4, 144.3, 143.2, 133.2, 131.4, 123.8, 122.8, 121.9, 120.8, 117.2, 117.0, 99.9, 97.6, 62.5, 55.9. HRMS *m/z* for $C_{20}H_{14}F_4N_4O_2$ $[M+H]^+$ Calcd. 419.1126. Found: 419.1123.

*3.1.3.12. 6-Methoxy-4-((1-(p-tolyl)-1H-1,2,3-triazol-4-yl)methoxy)-2-(trifluoromethyl)quinoline (**10l**).* White microcrystals, m.p. 181–183 °C, yield 65% (0.40 g). IR: ν_{max}/cm^{-1} 3138, 2927, 1578, 1505, 1482, 1378, 1232, 841, 722; ^1H NMR ($CDCl_3$) δ: 8.08 (s, 1H), 8.03 (d, $J = 9.0$ Hz, 1H), 7.61 (d, $J = 8.3$ Hz, 2H), 7.45–7.37 (m, 2H), 7.32 (d, $J = 8.2$ Hz, 2H), 7.26 (s, 1H), 5.55 (s, 2H), 3.91 (s, 3H), 2.42 (s, 3H). ^{13}C NMR ($CDCl_3$) δ: 161.3, 159.1, 146.8, 144.4, 142.9, 139.6, 134.7, 131.5, 130.6, 130.5, 123.9, 123.8, 122.9, 121.7, 120.9, 120.8, 100.0, 97.7, 62.6, 56.0, 21.4. HRMS *m/z* for $C_{21}H_{17}F_3N_4O_2$ $[M+H]^+$ Calcd. 415.1376. Found: 415.1377.

*3.1.3.13. 1-((1-(4-Methoxyphenyl)-1H-1,2,3-triazol-4-yl)methyl)-2-(trifluoromethyl)quinolin-4(1H)-one (**11a**).* Yellow microcrystals, m.p. 195–197 °C, yield 68% (0.41 g). IR: ν_{max}/cm^{-1} 3000, 2865, 1664, 1598, 1519, 1269, 1150, 830, 762, 740; ^1H NMR ($CDCl_3$) δ: 8.13 (d, $J = 8.6$ Hz, 1H), 8.02 (s, 1H), 7.84 (d, $J = 8.2$ Hz, 1H), 7.69 (t, $J = 7.9$ Hz, 1H), 7.56 (d, $J = 9.0$ Hz, 2H), 7.32 (t, $J = 7.7$ Hz, 1H), 7.12 (s, 1H), 6.96 (d, $J = 9.0$ Hz, 2H), 5.66 (s, 2H), 3.83 (s, 3H). ^{13}C NMR ($CDCl_3$) δ: 160.8, 160.2, 140.0, 138.1, 137.9, 132.4, 130.2, 126.0, 126.0, 123.5, 122.4, 121.5, 120.9, 120.8, 116.3, 115.6, 114.9, 114.9, 55.8, 38.9. HRMS *m/z* for $C_{20}H_{15}F_3N_4O_2$ $[M+H]^+$ Calcd. 401.1220. Found: 401.1196.

*3.1.3.14. 1-((1-(2-Methoxyphenyl)-1H-1,2,3-triazol-4-yl)methyl)-2-(trifluoromethyl)quinolin-4(1H)-one (**11b**).* White microcrystals, m.p. 184–186 °C, yield 79% (0.48 g). IR: ν_{max}/cm^{-1} 3138, 2980, 1662, 1598, 1483, 1235, 841, 770, 740; ^1H NMR ($CDCl_3$) δ: 8.23–8.16 (m, 2H), 7.84 (d, $J = 8.2$ Hz, 1H), 7.69 (dd, $J = 17.1$, 8.6 Hz, 2H), 7.38 (dd, $J = 11.1$, 4.7 Hz, 1H), 7.32 (t, $J = 7.7$ Hz, 1H), 7.11 (s, 1H), 7.07–6.98 (m, 2H), 5.68 (s, 2H), 3.84 (s, 3H). ^{13}C NMR ($CDCl_3$) δ: 170.8, 160.6, 151.1, 142.4, 139.9, 137.8, 137.5, 132.1, 130.3, 126.0, 125.7, 125.4, 123.3, 121.4, 120.8, 116.4, 115.4, 112.3, 56.0, 38.7. HRMS *m/z* for

$C_{20}H_{15}F_3N_4O_2$ $[M+H]^+$ Calcd. 401.1220. Found: 401.1214.

3.1.3.15. 1-((1-(2-Methoxyphenyl)-1H-1,2,3-triazol-4-yl)methyl)-6-methyl-2-(trifluoromethyl)quinolin-4(1H)-one ***(11c)***. Yellow microcrystals, m.p. 216–218 °C, yield 60% (0.37 g). IR: ν_{max}/cm^{-1} 3100, 2981, 1664, 1600, 1599, 1512, 1441, 1325, 1254, 830, 748; ^1H NMR ($CDCl_3$) δ: 8.19 (s, 1H), 8.08–8.03 (m, 1H), 7.66 (d, $J = 7.7$ Hz, 1H), 7.60 (s, 1H), 7.51 (d, $J = 8.6$ Hz, 1H), 7.37 (dd, $J = 12.5$, 4.9 Hz, 1H), 7.08 (s, 1H), 7.06–6.97 (m, 2H), 5.66 (s, 2H), 3.83 (s, 3H), 2.42 (s, 3H). ^{13}C NMR ($CDCl_3$) δ: 160.6, 151.3, 138.2, 133.5, 133.1, 133.1, 131.1, 130.9, 130.4, 128.0, 127.9, 126.3, 125.6, 121.3, 120.9, 116.3, 115.6, 112.4, 56.2, 38.8, 21.1. HRMS *m/z* for $C_{21}H_{17}F_3N_4O_2$ $[M+H]^+$ Calcd. 415.1330. Found: 415.1331.

3.1.3.16. 4-(2-(1-(4-Methoxyphenyl)-1H-1,2,3-triazol-4-yl)ethoxy)-2-(trifluoromethyl)-1,4-dihydroquinoline ***(12a)***. Yellow microcrystals, m.p. 158–160 °C, yield 76% (0.46 g). IR: ν_{max}/cm^{-1} 3100, 2980, 1575, 1516, 1364, 1250, 838, 767, 725; ^1H NMR ($CDCl_3$) δ: 8.20 (d, $J = 8.2$ Hz, 1H), 8.10 (d, $J = 8.2$ Hz, 1H), 7.82 (s, 1H), 7.74 (t, $J = 7.1$ Hz, 1H), 7.60–7.52 (m, 3H), 7.05 (s, 1H), 6.96 (d, $J = 8.3$ Hz, 2H), 4.60 (t, $J = 5.5$ Hz, 2H), 3.82 (s, 3H), 3.46 (t, $J = 5.5$ Hz, 2H). ^{13}C NMR ($CDCl_3$) δ: 162.9, 160.1, 149.7, 149.4, 149.2, 148.4, 144.4, 131.2, 130.7, 130.0, 127.8, 122.4, 121.9, 121.9, 120.6, 120.4, 115.0, 97.1, 68.1, 55.8, 26.0. HRMS *m/z* for $C_{21}H_{17}F_3N_4O_2$ $[M+H]^+$ Calcd. 415.1376. Found: 415.1362.

3.1.3.17. 6-Fluoro-4-(2-(1-(4-fluorophenyl)-1H-1,2,3-triazol-4-yl) ethoxy)-2-(trifluoromethyl)-1,4-dihydroquinoline ***(12b)***. Yellow microcrystals, m.p. 163–165 °C, yield 66% (0.40 g). IR: ν_{max}/cm^{-1} 3100, 2980, 1598, 1514, 1477, 1411, 1226, 841, 801, 742; ^1H NMR ($CDCl_3$) δ: 8.11 (dd, $J = 9.1$, 5.2 Hz, 1H), 7.87 (s, 1H), 7.76 (dd, $J = 9.1$, 2.3 Hz, 1H), 7.68–7.65 (m, 2H), 7.51 (t, $J = 8.6$ Hz, 1H), 7.2–7.17 (m, 2H),7.07 (s, 1H), 4.63 (t, $J = 6.4$ Hz, 2H), 3.47 (t, $J = 6.4$ Hz, 2H). ^{13}C NMR ($CDCl_3$) δ: 163.6, 162.4, 161.7, 160.4, 145.4, 144.6, 133.5, 132.6, 132.6, 122.8, 121.5, 121.3, 120.4, 117.1, 116.9, 106.0, 105.8, 97.5, 68.1, 26.0. HRMS *m/z* for $C_{20}H_{13}F_5N_4O$ $[M+H]^+$ Calcd. 421.1082. Found: 421.1066.

3.1.3.18. 6-Fluoro-4-(2-(1-(4-methoxyphenyl)-1H-1,2,3-triazol-4-yl) ethoxy)-2-(trifluoromethyl)-1,4-dihydroquinoline ***(12c)***. Yellow microcrystals, m.p. 158–160 °C, yield 78% (0.47 g). IR: ν_{max}/cm^{-1} 3100, 2980, 1596, 1517, 1479, 1373, 1273, 837, 743; ^1H NMR ($CDCl_3$) δ: 8.18–8.00 (m, 1H), 7.82 (s, 1H), 7.77 (d, $J = 7.9$ Hz, 1H), 7.64–7.43 (m, 3H), 7.07 (s, 1H), 6.97 (d, $J = 8.0$ Hz, 2H), 4.61 (t, $J = 5.5$ Hz, 2H), 3.83 (s, 3H), 3.46 (t, $J = 5.5$ Hz, 2H). ^{13}C NMR ($CDCl_3$) δ: 162.5, 162.4, 160.4, 160.0, 145.3, 144.1, 132.6, 132.5, 130.6, 122.7, 122.4, 121.4, 121.2, 120.5, 115.0, 106.0, 105.8, 97.5, 68.2, 55.8, 26.0. HRMS *m/z* for $C_{21}H_{16}F_4N_4O_2$ $[M+H]^+$ Calcd. 433.1282. Found: 433.1263.

3.1.3.19. 6-Fluoro-4-(2-(1-(2-methoxyphenyl)-1H-1,2,3-triazol-4-yl) ethoxy)-2-(trifluoromethyl)-1,4-dihydroquinoline ***(12d)***. Yellow microcrystals, m.p 155–157 °C, yield 62% (0.38 g). IR: ν_{max}/cm^{-1} 3100, 2970, 1600, 1510, 1375, 1235, 840, 766; ^1H NMR ($CDCl_3$) δ: 8.12 (dd, $J = 9.2$, 5.2 Hz, 1H), 8.06 (s, 1H), 7.80–7.75 (m, 2H), 7.51 (td, $J = 9.2$, 2.7 Hz, 1H), 7.39 (t, $J = 7.9$ Hz, 1H), 7.12–6.97 (m, 3H), 4.63 (t, $J = 6.4$ Hz, 2H), 3.83 (s, 3H), 3.48 (t, $J = 6.4$ Hz, 2H). ^{13}C NMR ($CDCl_3$) δ: 162.6, 160.4, 151.2, 148.6, 145.3, 143.0, 132.6, 132.5, 131.0, 130.3, 125.6, 124.3, 121.5, 121.4, 121.2, 112.4, 105.9, 97.5, 68.3, 56.1, 26.0. HRMS *m/z* for $C_{21}H_{16}F_4N_4O_2$ $[M+H]^+$ Calcd. 433.1282. Found: 433.1262.

3.1.3.20. 4-(2-(1-(4-Methoxyphenyl)-1H-1,2,3-triazol-4-yl)ethoxy)-6-methyl-2-(trifluoromethyl)-1,4-dihydroquinoline ***(12e)***. Yellow microcrystals, m.p. 152–154 °C, yield 84% (0.51 g). IR: ν_{max}/cm^{-1} 3100, 2980, 1577, 1516, 1416, 1366, 1249, 829, 737, 715; ^1H NMR ($CDCl_3$) δ: 8.01 (d, $J = 8.6$ Hz, 1H), 7.96 (s, 1H), 7.81 (s, 1H), 7.69–7.50 (m, 3H), 7.04 (s, 1H), 6.98 (d, $J = 9.0$ Hz, 2H), 4.60 (t, $J = 6.6$ Hz, 2H), 3.84 (s, 3H), 3.48 (t, $J = 6.6$ Hz, 2H), 2.54 (s, 3H). ^{13}C NMR ($CDCl_3$) δ: 162.4, 160.1, 148.5, 148.2, 146.9, 144.4, 138.0, 133.4, 130.7, 129.7, 122.9, 122.4, 121.8, 121.8, 120.7, 120.4, 115.0, 97.1, 67.9, 55.8, 26.0, 22.1. HRMS *m/z* for $C_{22}H_{19}F_3N_4O_2$ $[M+H]^+$ Calcd. 429.1533. Found: 429.1526.

3.2. Biological studies

Details of biological studies are mentioned in the supplementary materials.

Declaration of Competing Interest

The authors declare that they have no known competing financial interests or personal relationships that could have appeared to influence the work reported in this paper.

Acknowledgments

We thank the Egyptian Cultural and Educational Bureau Scholarship. The authors also thank the Center for Undergraduate Research and Scholarship (CURS), Translational Research Program (TRP) at Augusta University and the Egyptian Academy of Scientific Research and Technology (ASRT) within the program under contract number 7303 for financial support.

Appendix A. Supplementary material

Supplementary data to this article can be found online at https://doi.org/10.1016/j.bioorg.2021.105117.

References

[1] H. Lu, C.W. Stratton, Y.-W. Tang, Outbreak of pneumonia of unknown etiology in Wuhan, China: the mystery and the miracle, J. Med. Virol. 92 (4) (2020) 401–402.
[2] Q. Li, X. Guan, P. Wu, X. Wang, L. Zhou, Y. Tong, R. Ren, K.S.M. Leung, E.H.Y. Lau, J.Y. Wong, X. Xing, N. Xiang, Y. Wu, C. Li, Q.i. Chen, D. Li, T. Liu, J. Zhao, M. Liu, W. Tu, C. Chen, L. Jin, R. Yang, Q.i. Wang, S. Zhou, R. Wang, H. Liu, Y. Luo, Y. Liu, G.e. Shao, H. Li, Z. Tao, Y. Yang, Z. Deng, B. Liu, Z. Ma, Y. Zhang, G. Shi, T.T. Y. Lam, J.T. Wu, G.F. Gao, B.J. Cowling, B.o. Yang, G.M. Leung, Z. Feng, Early transmission dynamics in Wuhan, China, of novel coronavirus-Infected pneumonia, N. Engl. J. Med. 382 (13) (2020) 1199–1207.
[3] N. Chen, M. Zhou, X. Dong, J. Qu, F. Gong, Y. Han, Y. Qiu, J. Wang, Y. Liu, Y. Wei, J. Xia, T. Yu, X. Zhang, L.i. Zhang, Epidemiological and clinical characteristics of 99 cases of 2019 novel coronavirus pneumonia in Wuhan, China: a descriptive study, Lancet 395 (10223) (2020) 507–513.
[4] World Health Organization, Clinical management of severe acute respiratory infection when novel coronavirus (nCoV) infection is suspected: interim guidance, 2020. https://www.who.int/emergencies/diseases/novel-coronavirus-2019/technical-guidance-publications.
[5] T.U. Singh, S. Parida, M.C. Lingaraju, M. Kesavan, D. Kumar, R.K. Singh, Drug repurposing approach to fight COVID-19, Pharmacol Rep. 72 (6) (2020) 1479–1508.
[6] S. Dotolo, A. Marabotti, A. Facchiano, R. Tagliaferri, A review on drug repurposing applicable to COVID-19, briefings in bioinformatics, 2020, bbaa288. https://doi.org/10.1093/bib/bbaa288.
[7] S. Xiu, A. Dick, H. Ju, S. Mirzaie, F. Abdi, S. Cocklin, P. Zhan, X. Liu, Inhibitors of SARS-CoV-2 entry: Current and future opportunities, J. Med. Chem. 63 (21) (2020) 12256–12274.
[8] X. Yao, F. Ye, M. Zhang, C. Cui, B. Huang, P. Niu, X.u. Liu, L.i. Zhao, E. Dong, C. Song, S. Zhan, R. Lu, H. Li, W. Tan, D. Liu, In vitro antiviral activity and projection of optimized dosing design of hydroxychloroquine for the treatment of severe acute respiratory syndrome coronavirus 2 (SARS-CoV-2), Clin. Infect. Dis. ciaa237. 71 (15) (2020) 732–739.
[9] C.-Y. Chen, F.-L. Wang, C.-C. Lin, Chronic hydroxychloroquine use associated with qt prolongation and refractory ventricular arrhythmia, Clin. Toxicol. 44 (2) (2006) 173–175.
[10] P. Stas, D. Faes, P. Noyens, Conduction disorder and QT prolongation secondary to long-term treatment with chloroquine, Int. J. Cardiol. 127 (2008) e80–e82.
[11] S.A. Yaylali, F. Sadigov, H. Erbil, A. Ekinci, A.A. Akcakaya, Chloroquine and hydroxychloroquine retinopathy-related risk factors in a turkish cohort, Int. Ophthalmol. 33 (6) (2013) 627–634.
[12] R. Musharrafieh, N. Kitamura, Y. Hu, J. Wang, Development of broad-spectrum enterovirus antivirals based on quinoline scaffold, Bioorg. Chem. 101 (2020) 103981, https://doi.org/10.1016/j.bioorg.2020.103981.

[13] A. Ali, N. Sepay, M. Afzal, N. Sepay, A. Alarifi, M. Shahid, M. Ahmad, Molecular designing, crystal structure determination and in silico screening of copper(II) complexes bearing 8-hydroxyquinoline derivatives as anti-COVID-19, Bioorg. Chem. 110 (2021) 104772, https://doi.org/10.1016/j.bioorg.2021.104772.
[14] M.B. Alshammari, M. Ramadan, A.A. Aly, E.M. El-Sheref, M.A. A. Ibrahim, A.M. Shawky, Synthesis of potentially new schiffbases of N -substituted-2-quinolonylacetohydrazides as anti-COVID-19 agents, J. Mol. Struct. 1230 (2021) 129649, https://doi.org/10.1016/j.molstruc.2020.129649.
[15] A.A. Aly, A.A. Hassan, A.H. Mohamed, E.M. Osman, S. Bräse, M. Nieger, M.A. A. Ibrahim, S.M. Mostafa, Synthesis of 3,3′-methylenebis(4-hydroxyquinolin-2 (1H)-ones) of prospective anti-COVID-19 drugs, Mol. Div. 25 (1) (2021) 461–471.
[16] D. Kumar, G. Chauhan, S. Kalra, B. Kumar, M.S. Gill, A perspective on potential target proteins of COVID-19: Comparison with SARS-CoV for designing new small molecules, Bioorg. Chem. 104 (2020), 104326.
[17] J. Loschwitz, A. Jaeckering, M. Keutmann, M. Olagunju, R.J. Eberle, M. A. Coronado, O.O. Olubiyi, B. Strodel, Novel inhibitors of the main protease enzyme of SARS-CoV-2 identified via molecular dynamics simulation-guided in vitro assay, Bioorg. Chem. 111 (2020), 104862.
[18] S. Guo, H. Xie, Y. Lei, B. Liu, L. Zhang, Y. Xu, Z. Zuo, Discovery of novel inhibitors against main protease (Mpro) of SARS-CoV-2 via virtual screening and biochemical evaluation, Bioorg. Chem. 110 (2020), 104767.
[19] L.-Y. Sun, C. Chen, J. Su, J.-Q. Li, H. Gao, J.-Z. Chigan, H.-H.L. Zhai, K.-W. Yang, Ebsulfur and Ebselen as highly potent scaffolds for the development of potential SARS-CoV-2 antivirals, Bioorg. Chem. 112 (2020) 104889.
[20] F.X. Dominguez-Villa, N.A. Duran-Iturbide, J.G. Avila-Zarraga, Synthesis, molecular docking, and in silico ADME/Tox profiling studies of new 1-aryl-5-(3-azidopropyl)indol-4-ones: Potential inhibitors of SARS CoV-2 main protease, Bioorg. Chem. 106 (2020), 104497.
[21] Siva S Panda, Adel S Girgis, Hitesh H Honkanadavar, Riham F George, Aladdin M Srour, Synthesis of new ibuprofen hybrid conjugates as potential anti-inflammatory and analgesic agents, Future Med. Chem. 12 (15) (2020) 1369–1386.
[22] Siva S. Panda, Adel S. Girgis, Sean J. Thomas, Jason E. Capito, Riham F. George, Asmaa Salman, May A. El-Manawaty, Ahmed Samir, Synthesis, pharmacological profile and 2D-QSAR studies of curcumin-amino acid conjugates as potential drug candidates, Eur. J. Med. Chem. 196 (2020) 112293, https://doi.org/10.1016/j.ejmech.2020.112293.
[23] Israa A. Seliem, Siva S. Panda, Adel S. Girgis, Yosra I. Nagy, Riham F. George, Walid Fayad, Nehmedo G. Fawzy, Tarek S. Ibrahim, Amany M.M. Al-Mahmoudy, Rajeev Sakhuja, Zakaria K.M. Abdel-samii, Design, synthesis, antimicrobial, and DNA gyrase inhibitory properties of fluoroquinolone-dichloroacetic acid hybrids, Chem. Biol. Drug Des. 95 (2) (2020) 248–259.
[24] S.S. Panda, A.S. Girgis, B.B. Mishra, M. Elagawany, V. Devarapalli, W.F. Littlefield, A. Samir, N.G. Fawzy, A.M. Srour, Novel pyrazinoic acid-isoniazid conjugates with amino acid linker: Microwave assisted synthesis, anti-infective properties, and molecular modeling studies, RSC Adv. 9 (35) (2019) 20450–20462.
[25] Hassan M. Faidallah, Adel S. Girgis, Anand D. Tiwari, Hitesh H. Honkanadavar, Sean J. Thomas, Ahmed Samir, Atef Kalmouch, Khalid A. Alamry, Khalid A. Khan, Tarek S. Ibrahim, Amany M.M. AL-Mahmoudy, Abdullah M. Asiri, Siva S. Panda, Synthesis, antibacterial properties and 2D-QSAR studies of quinolone-triazole conjugates, Eur. J. Med. Chem. 143 (2018) 1524–1534.
[26] Hassan M. Faidallah, Siva S. Panda, Juan C. Serrano, Adel S. Girgis, Khalid A. Khan, Khalid A. Alamry, Tanya Therathanakorn, Marvin J. Meyers, Francis M. Sverdrup, Christopher S. Eickhoff, Stephen G. Getchell, Alan R. Katritzky, Synthesis, antimalarial properties and 2D-QSAR studies of novel triazole-quinine conjugates, Bioorg. Med. Chem. 24 (16) (2016) 3527–3539.
[27] Bo Zhang, Comprehensive review on the anti-bacterial activity of 1,2,3-triazole hybrids, Eur. J. Med. Chem. 168 (2019) 357–372.
[28] Dae-Kee Kim, Joonseop Kim, Hyun-Ju Park, Synthesis and biological evaluation of novel 2-pyridinyl[1,2,3]triazoles as inhibitors of transforming growth factor β1 type 1 receptor, Bioorg. Med. Chem. Lett. 14 (10) (2004) 2401–2405.
[29] Matthew Whiting, Jonathan C. Tripp, Ying-Chuan Lin, William Lindstrom, Arthur J. Olson, John H. Elder, K. Barry Sharpless, Valery V. Fokin, Rapid discovery and structure-activity profiling of novel inhibitors of human immunodeficiency virus type 1 protease enabled by the copper(I)-catalyzed synthesis of 1,2,3-triazoles and their further functionalization, J. Med. Chem. 49 (26) (2006) 7697–7710.
[30] Z.-Y. Cheng, W.-J. Li, F. He, J.-M. Zhou, X.-F. Zhu, Synthesis and biological evaluation of 4-aryl-5-cyano-2*H*-1,2,3-triazoles as inhibitor of HER2 tyrosine kinase, Bioorg. Med. Chem. 15 (3) (2007) 1533–1538.
[31] Fernando de C. da Silva, Maria Cecilia B.V. de Souza, Izabel I.P. Frugulhetti, Helena C. Castro, Silmara L. de O. Souza, Thiago Moreno L. de Souza, Diego Q. Rodrigues, Alessandra M.T. Souza, Paula A. Abreu, Fabiana Passamani, Synthesis, HIV-RT inhibitory activity and SAR of 1-benzyl-1*H*-1,2,3-triazole derivatives of carbohydrates, Eur. J. Med. Chem. 44 (1) (2009) 373–383.
[32] N.A. Meanwell, Fluorine and fluorinated motifs in the design and application of bioisosteres for drug design, J. Med. Chem. 61 (14) (2018) 5822–5880.
[33] Siva S. Panda, Subhash C. Jain, New trifluoromethyl quinolone derivatives: Synthesis and investigation of antimicrobial properties, Bioorg. Med. Chem. Lett. 23 (11) (2013) 3225–3229.
[34] S. Maracic, J. Lapic, S. Djakovic, T. Opacak-Bernardi, L. Glavas-Obrovac, V. Vrcek, S. Raic-Malic, Quinoline and ferrocene conjugates: Synthesis, computational study and biological evaluations, Appl. Organometal Chem. 33 (1) (2019), e4628.
[35] Maria Feoktistova, Peter Geserick, Martin Leverkus, Crystal violet assay for determining viability of cultured cells, Cold Spring Harb Protoc 2016 (4) (2016), https://doi.org/10.1101/pdb.prot087379.
[36] A. Mostafa, A. Kandeil, Y.A.M.M. Elshaier, O. Kutkat, Y. Moatasim, A.A. Rashad, M. Shehata, M.R. Gomaa, N. Mahrous, S.H. Mahmoud, M. GabAllah, H. Abbas, A. El Taweel, A.E. Kayed, M.N. Kamel, M. El Sayes, D.B. Mahmoud, R. El-Shesheny, G. Kayali, M.A. Ali, FDA-approved drugs with potent in vitro antiviral activity against severe acute respiratory syndrome coronavirus 2, Pharmaceuticals 13 (12) (2020) 443.
[37] Radwan Alnajjar, Ahmed Mostafa, Ahmed Kandeil, Ahmed A. Al-Karmalawy, Molecular docking, molecular dynamics, and in vitro studies reveal the potential of angiotensin II receptor blockers to inhibit the COVID-19 main protease, Heliyon 6 (12) (2020) e05641, https://doi.org/10.1016/j.heliyon.2020.e05641.
[38] http://www.rcsb.org/structure/6LU7.
[39] Zhenming Jin, Xiaoyu Du, Yechun Xu, Yongqiang Deng, Meiqin Liu, Yao Zhao, Bing Zhang, Xiaofeng Li, Leike Zhang, Chao Peng, Yinkai Duan, Jing Yu, Lin Wang, Kailin Yang, Fengjiang Liu, Rendi Jiang, Xinglou Yang, Tian You, Xiaoce Liu, Xiuna Yang, Fang Bai, Hong Liu, Xiang Liu, Luke W. Guddat, Wenqing Xu, Gengfu Xiao, Chengfeng Qin, Zhengli Shi, Hualiang Jiang, Zihe Rao, Haitao Yang, Structure of M^{pro} from SARS-CoV-2 and discovery of its inhibitors, Nature 582 (7811) (2020) 289–293.